SECURITY INFORMATION

Copy
RM L53G10a

NACA RM L53G10a

TECH LIBRARY KAFB, NM
0144389

NACA

RESEARCH MEMORANDUM

INVESTIGATION OF WING FLUTTER AT TRANSONIC SPEEDS FOR SIX SYSTEMATICALLY VARIED WING PLAN FORMS

By George W. Jones, Jr., and Hugh C. DuBose

Langley Aeronautical Laboratory
Langley Field, Va.

manner to

NATIONAL ADVISORY COMMITTEE
FOR AERONAUTICS

WASHINGTON

August 13, 1953

Classification cancelled or changed to UNCLASSIFIED

By Authority of NASA Tech Pub Announcement #18

(OFFICER AUTHORIZED TO CHANGE)

By ..... 16 Aug 67

NAME AND

GRADE OF OFFICER MAKING CHANGE)

31 Mar 61

DATE

TECH LIBRARY KAFB, NM
0144389

1W

NATIONAL ADVISORY COMMITTEE FOR AERONAUTICS

RESEARCH MEMORANDUM

INVESTIGATION OF WING FLUTTER AT TRANSONIC SPEEDS FOR SIX SYSTEMATICALLY VARIED WING PLAN FORMS

By George W. Jones, Jr., and Hugh C. DuBose

SUMMARY

An investigation of the effects of systematic variations in wing plan form on the flutter speed at Mach numbers between 0.73 and 1.43 has been conducted in the 26-inch Langley transonic blowdown tunnel. The angle of sweepback was varied from 0° to 60° on wings of aspect ratio 4, and the aspect ratio was varied from 2 to 6 on wings with 45° of sweepback. The results are presented as ratios between the experimental flutter speed and the reference flutter speed calculated on the basis of incompressible two-dimensional flow. This ratio, designated as the flutter-speed ratio, is plotted as a function of Mach number for the various wings. It is found that the flutter-speed ratio increased rapidly past sonic speed for sweep angles of 45° and less, indicating a favorable effect of Mach number. For sweepback of 60°, the flutter-speed ratio was nearly constant throughout the Mach number range of the tests. Reducing the aspect ratio had a favorable effect on the flutter-speed ratio which was of the order of 100 percent higher for the aspect-ratio-2 wing than for the aspect-ratio-6 wing. This percentage difference was nearly constant throughout the Mach number range, indicating that the effect of Mach number was about the same for all aspect ratios tested.

INTRODUCTION

There is an urgent need for experimental data dealing with the problem of wing flutter in the transonic speed range. In order to provide a portion of the needed information, several flutter investigations have been undertaken in the Langley transonic blowdown tunnel. The results of the first of these investigations are presented in reference 1 and show that reliable flutter data can be obtained from a slotted-throat transonic tunnel. In the present investigation, the flutter characteristics of a series of six systematically varied high-speed wing plan forms were studied at transonic speeds. The purpose of the investigation was to determine the effects of sweepback and aspect ratio on the flutter speed for Mach numbers in the vicinity of 1.0.

NASA 55-2048

The flutter tests were made at 0° angle of attack over a range of Mach numbers from 0.73 to 1.43. The systematic plan-form variation was accomplished by varying the sweepback from 0° to 60° on wings with an aspect ratio of 4 and varying the aspect ratio from 2 to 6 on wings with a sweepback of 45°. The results of the investigation are presented and analyzed herein.

SYMBOLS

A	aspect ratio including body intercept
a	distance in wing semichords from midchord to elastic-axis position measured positive rearward, $2x_o - 1$
A_g	geometric aspect ratio of one wing panel, $\frac{\text{Exposed half-span}}{\text{Mean streamwise chord}}$
b	half-chord perpendicular to quarter-chord line, ft
b_r	half-chord perpendicular to quarter-chord line at intersection of quarter-chord line and wing root (except for 245 wing, see "Methods of Analysis"), ft
b_s	half-chord measured streamwise at intersection of wing root and fuselage, ft
c	wing chord measured perpendicular to quarter-chord line, ft
f_{h_1}	first bending natural frequency, cps
f_{h_2}	second bending natural frequency, cps
f_t	first torsion natural frequency, cps
f_α	uncoupled first torsion frequency relative to elastic axis, $f_t\left[1 - \frac{(x_\alpha/r_\alpha)^2}{1 - \left(f_{h_1}/f_t\right)^2}\right]^{1/2}$, cps
g	structural damping coefficient
g_h	structural damping coefficient for bending vibration
g_α	structural damping coefficient for torsional vibration

I_α	polar moment of inertia of wing section about elastic axis, slug-ft^2/ft
k	reduced-frequency parameter, $\omega b/V$
l	length of wing panels, outside fuselage, measured along quarter-chord line (except for 245 wing, see "Methods of Analysis"), ft
M	Mach number
m	mass of wing per unit length along quarter-chord line, slugs/ft
q	dynamic pressure, lb/sq ft
r_α	nondimensional radius of gyration of wing section about elastic axis, $\left(I_\alpha/mb^2\right)^{1/2}$
V	stream velocity at flutter, fps
V'	stream velocity at flutter estimated for $\mu = 50$, fps
V_n	component of stream velocity at flutter, normal to quarter-chord line, fps
V_e/V_R	flutter-speed ratio
x_o	distance of elastic axis of wing section behind leading edge, fraction of chord
x_α	distance in semichords from wing-elastic-axis position to wing center-of-gravity position
η	nondimensional coordinate along quarter-chord line (except for 245 wing, see "Methods of Analysis"), fraction of length l
μ	ratio of mass of wing to mass of a cylinder of air of diameter equal to chord of wing, both taken for equal length along quarter-chord line, $m/\pi\rho b^2$
λ	taper ratio, Tip chord /Chord in plane of symmetry
Λ	angle of sweepback of quarter-chord line, deg
ρ	air density, slugs/cu ft

ω angular frequency of vibration, radians/sec

ω_h angular bending frequency, radians/sec

ω_α angular uncoupled torsion frequency about elastic axis, radians/sec

Subscripts:

e experimental values at start of flutter

R calculated values based on two-dimensional incompressible-flow theory with account taken of mode shape and sweep (corresponds to subscript Λ in ref. 2)

stnd. based on sea-level conditions

APPARATUS AND TESTS

Wind tunnel.- The 26-inch Langley transonic blowdown tunnel is equipped with a slotted test section, octagonal in shape, which allows the tunnel to operate through the transonic speed range from subsonic Mach numbers up to a Mach number of approximately 1.45. A plan view of the tunnel, with a model installed, and a cross-sectional view of the octagonal test section are shown in figure 1.

A variable and continuous regulation of the air flow is allowed by a set of plug valves, located between a high-pressure reservoir and the tunnel, and operated by a single control. A quick-operating mechanism closes the valves in approximately 1/2 second.

Orifice plates of different sizes may be installed downstream of the test section. The orifice, when choked, permits a prescribed test-section Mach number to be maintained while stagnation pressure (and thus density) is varied from that for orifice choke up to about 75 lb/sq in. Since the occurrence of flutter depends on air density as well as velocity and Mach number, this technique permits flutter to be obtained at several Mach numbers on the same model by the simple process of varying the tunnel pressure. The tunnel air temperature varies with initial reservoir conditions and expansion in the reservoir during each run. The test-section velocity is therefore not uniquely defined by the Mach number.

Support system.- The wings were mounted at 0° angle of attack on a 3-inch-diameter cylindrical sting fuselage. A fixed wing root condition was obtained by mounting the wing with close-fitting filler blocks and four 3/8-inch bolts. Figure 2 shows a flutter model mounted on the sting

fuselage. The fuselage nose was extended into the subsonic flow region of the tunnel entrance cone in order to prevent the formation of a bow shock wave which might reflect on the model. The support system was considered to form a rigid mount for the wings since the mass of the support system was very large when compared to the mass of a wing.

Instrumentation.- Each model was instrumented with wire strain gages located on the wing near the root and so oriented that the output of the gages indicated the wing bending and torsion deflections. The primary use of the strain gages was to provide an indication of the start of flutter and to obtain a record of the frequency of wing bending and torsion oscillations. Some estimates of the magnitude of the deflections and the phase angle between bending and torsion could also be obtained from the output of the strain gages.

During the tests a multichannel recording oscillograph was used to make recordings of the strain-gage signals, tunnel stagnation pressure and temperature, and test-section static pressure. A sample test record is given in figure 3 in which the start of flutter is shown by the change in wing oscillations from a random form to a sine wave, the amplitude of which rapidly increases.

A high-speed 16-mm motion-picture camera (approximately 1,000 frames per second) was used to obtain a visual record of wing deflection during flutter. These films served as a supplement to visual observation of the mode shape and magnitude of flutter.

Tests.- The objectives of the wind-tunnel test program were to determine the flutter speed and flutter frequency of each wing at 0° angle of attack for several Mach numbers in the transonic range. The procedure followed in obtaining model flutter at a particular Mach number was to increase the stagnation pressure gradually until flutter was seen by an observer looking through a porthole in the side of the tunnel. The stagnation pressure and Mach number were then held constant for a few seconds at initial flutter conditions, after which the air flow was quickly stopped in an effort to save the model from destruction by flutter.

MODELS

Model description.- Flutter tests were conducted on six high-speed wing plan forms which had systematic variations of sweepback and aspect ratio. The other geometric parameters were held constant. Four of the wings had an aspect ratio of 4 and angles of sweepback of the quarter-chord line of 0°, 45°, 52.5°, and 60°. The other two wings had sweepback of the quarter-chord line of 45° and aspect ratios of 2 and 6. All the wings had NACA 65A004 streamwise airfoil sections, a taper ratio of

0.6, and a ratio of body-cross-section area to wing-plan-form area of 0.15. The model spans were 0.808 foot, 1.14 feet, and 1.40 feet for the wings of aspect ratio 2, 4, and 6, respectively. Drawings of the various plan forms tested are presented in figure 4. Each plan form is designated by a three-digit number; the first digit gives the aspect ratio and the last two digits give the angle of sweepback.

It was necessary to employ various materials and types of construction in the models so that flutter could be obtained within the range of air densities available in the transonic blowdown tunnel. In general, wings having the higher length-chord ratios required stiffer structures. The 400 and 445 wings were made of solid compreg (a laminated, compressed, resin-impregnated maple). The 452 wing was made of compreg with a 0.006-inch sheet of Fiberglas wrapped around the outside and bonded to the wood; the 460 wing was constructed similar to the 452 wing except that the thickness of the Fiberglas was 0.018 inch. In the construction of the 452 and 460 wings, an attempt was made to undercut the wood before wrapping the wings with Fiberglas; however, the airfoil shapes that resulted had an average maximum thickness of 5 percent of the streamwise chord rather than the intended 4 percent. The 245 wing had a tapered spar of pine 2 percent thick, with grain direction parallel to the quarter-chord line. This spar was sandwiched between two layers of balsa 1 percent thick with grain direction parallel to the airstream. The 645 wing was made of solid magnesium.

Physical parameters.- Measurements were made of the following physical parameters: elastic-axis location, first and second bending and first torsion natural frequencies, mass variations along the span, moment-of-inertia variation along the span, center-of-gravity location, and the structural damping coefficient in bending. A brief discussion of the methods used to obtain the measurements follows.

For the determination of the elastic axis, the wings were clamped along a line perpendicular to the quarter-chord line and passing through the intersection of the wing trailing edge and the root. At several spanwise stations, the wings were loaded at a number of points along a line perpendicular to the quarter-chord line. The chordwise position of load application, for which no rotation of the line perpendicular to the quarter-chord line occurred, was determined. A straight line faired through these flexural centers was taken to be the elastic axis. An exception was the 245 wing which was clamped at the root in a streamwise direction. It was impractical to clamp the 245 wing in the same manner as the other wings because of the small length-chord ratio. This change in clamping caused the elastic axis to shift rearward with the result that the values of the elastic-axis location and the radius of gyration for the 245 wing were greatly different from those of the other plan forms.

The frequencies of the pertinent natural modes of each wing were determined with the wings clamped at the root in a streamwise direction which corresponded to the wing mounting during the tests. The several methods used to determine natural frequencies were:

(1) Analysis of the sound response obtained by striking the wing. In this method, the natural frequency was obtained by striking the wing and tuning the sound analyzer for maximum response. The node line for a particular mode could be detected by the occurrence of a minimum response in that mode when the point of striking coincided with a point on the node line.

(2) Detection of resonant frequencies with a vibrator applied at the wing root. The technique employed in this method involved the use of sand to reveal node lines and indicate the corresponding resonant frequencies of the vibrating wing.

(3) The use of the wing strain gages to measure the frequencies of the decaying oscillations following release of the wing tip from a deflected position.

(4) For the determination of the lower first bending frequencies only, the observation of vibrations under stroboscopic lighting.

Difficulty was experienced in defining the frequency of the first torsional modes of both the 445 wing and the 452 wing. For the case of the 445 wing, three resonant torsional frequencies were found in the same range, two of which had equal response but node lines near the leading and trailing edge, respectively. The third mode had a slightly weaker response but a node line nearly parallel to the quarter-chord line and just forward of the midchord line. For the 452 wing, a response of almost uniform amplitude over a range of frequencies was obtained. For both wings, the frequency corresponding to the node line most nearly parallel to the quarter-chord line was taken to be the first coupled torsion frequency. In all cases, the uncoupled torsion frequency was obtained from the relation given in reference 2 and included in the list of symbols herein. The uncoupled bending frequency was taken to be the same as the measured first bending frequency. It was found that, for the wings tested, differences in frequencies between left and right wing panels and between two models of the same design were smaller than the accuracy with which the frequency was measured. Therefore, only one value of the bending and torsion frequencies is presented for each wing.

A model of each plan form was cut into strips perpendicular to the quarter chord and approximately 0.5 inch in width. The number of strips varied from 3 on the 245 wing to 11 on the 645 wing. The variation of mass per unit length along the span was found by weighing the strips. The variation of moment of inertia along the span was found by swinging

[redacted]

the strips in a calibrated torsion pendulum about an axis coinciding with the wing elastic axis. The section center-of-gravity location was determined by balancing the strips on a knife edge held parallel to the quarter-chord line.

The structural damping coefficients in bending were found by taking the logarithmic decrement of the bending strain-gage traces after the wing was depressed at the tip and released. These measurements were made in air.

Values of the parameters describing the geometric and physical properties of the models can be found in tables I and II. The ranges of variation of some of the more important parameters are: center-of-gravity 0.44c to 0.46c, ratio of first bending to first torsion frequencies squared 0.0083 to 0.420, and structural damping coefficient in first bending 0.013 to 0.030.

METHODS OF ANALYSIS

The purpose of this investigation is to show the effect of changes in wing plan form on the flutter speed in the transonic range. Because of the manner in which the experimental investigation was made, however, the value of the mass-density parameter μ varied for the different Mach numbers at which flutter was obtained on the various wings. Furthermore, the value of the torsional frequency ω_α, as well as the nondimensional quantities x_α, a, r_α, and ω_h/ω_α, varied for the different wing plan forms. Consequently, a true indication of the effects of plan form and Mach number cannot be obtained merely from a comparison of the experimentally determined flutter speeds. In an effort to separate the effects of plan-form variations from the effects of the other variables, the results will be presented in the form of a ratio of the experimental flutter speed to a calculated flutter speed V_e/V_R where V_R is the calculated reference flutter speed and V_e is the experimental flutter speed. The method for obtaining the reference flutter speed will now be discussed briefly.

Reference flutter speed.- The reference flutter speed as computed in the analysis is based on two-dimensional incompressible-flow aerodynamic coefficients. The method used for calculation of V_R was an application of that given in reference 2 (V_R corresponds to V_Λ in ref. 2). The terms in the analysis which involved the spanwise derivative of the velocity potential (bracketed terms in ref. 2) were omitted. Except in the case of the 245 wing, the effective wing root and tip are defined in the present analysis as the perpendiculars to the quarter-chord line at the intersections of the quarter-chord line with the actual root and tip, respectively. In the case of the 245 wing, the effective root is defined

as the perpendicular to the elastic axis at the intersection of the elastic axis and the root, and the effective tip is defined as the perpendicular to the elastic axis drawn through the intersection of the half-chord line and the wing tip. In all cases, the root semichord b_r is one-half the effective root chord; and the length l is the length of the effective wing panel, that is, the perpendicular distance between the effective root and the effective tip.

Two modes were used in the analysis. The frequencies used were the measured first bending frequency and the uncoupled first torsion frequency. The mode shape of the wings during flutter was represented in the analysis by the first bending and first torsion mode shapes of a uniform cantilever beam. The mode shapes of a uniform beam were thought to approximate the flutter mode shape with a sufficient degree of accuracy and were employed in preference to the mode shapes of a tapered beam as a matter of convenience. There were two indications, however, that higher natural modes than the first should perhaps have been included in the calculations for the wings having the higher length-chord ratios. High-speed camera results indicated, as will be discussed later, an outward displacement toward the tip of the region of maximum curvature of the flutter mode shape for these wings. This suggests the presence of higher mode shapes than the first, particularly in bending, in the flutter mode. Also for the higher length-chord-ratio wings, namely the 452, 460, and 645 wings, the flutter frequency was near the second natural bending frequency which in turn was less than the first torsion frequency.

The values of k were weighted along the span in accordance with the chord variation. The spanwise variation of the Theodorsen functions $F(k)$ and $G(k)$ were approximated by a linear variation between their root and tip values. With the Theodorsen functions represented in this manner, it was possible to set up the analysis so that computation of the flutter determinant coefficients and solution of the determinant could be accomplished quite rapidly by automatic, punchcard computing equipment. A comparison of the results obtained on the automatic equipment using the linear variation of $F(k)$ and $G(k)$ with those by manual methods using the actual values of $F(k)$ and $G(k)$ at 10 points along the span showed excellent agreement.

The solution of the flutter stability determinant was carried out in such a way that a curve of structural damping coefficient g against $V_n/b_r\omega_\alpha$ was obtained for each air density. Two such curves are shown in figure 5. The smooth curve designated "Typical 400 wing curve" is typical of most flutter experience. On this curve, an increase in damping from a value of zero results in an increase in V_R since V_R varies directly with V_n. A common practice when the curves of g are of this type is to present V_R values based on a structural-damping value of zero which gives a value of V_R that is conservative when compared with values based on actual damping. In the present analysis, a type of curve

frequently encountered is shown by the "S" shaped curve in figure 5 designated "Typical 445 wing curve." Examination of this curve shows that an increase in damping from a zero value results in a decrease in V_R. If zero damping is assumed in this case, the value of V_R obtained is unconservative when compared with a value based on the actual damping. For this reason, the values of V_R employed herein are based on the measured value of the structural damping. Since only the structural damping in bending was measured, it was assumed that $g_h = g_\alpha = g$.

Flutter-speed coefficient.- In order to provide some indication of the manner in which the actual flutter speed might be expected to vary with wing plan form and Mach number for wings having a constant value of the density-ratio parameter μ, a flutter-speed coefficient $V'/b_s\omega_\alpha$ was determined from the theoretical and experimental data.

The parameter $V'/b_s\omega_\alpha$ was determined as follows: The theoretical value of the flutter-speed coefficient $V_R/b_s\omega_\alpha$, corresponding to a value of the relative-density parameter μ of 50, was determined for each of the wings tested from the data given in tables I and III. In order to obtain values of $V_R/b_s\omega_\alpha$ corresponding to a μ of 50 for the 245, 460, and 400 wings, it was necessary to extrapolate the straight lines given by plots of $V_R/b_s\omega_\alpha$ against $\sqrt{\mu}$. On the basis of the assumption that the curves of V_e/V_R are independent of μ, the theoretical value of $V_R/b_s\omega_\alpha$ for each wing was corrected by use of the values of V_e/V_R as multipliers. The products obtained by this procedure are the values of $V'/b_s\omega_\alpha$ which will be presented as a function of Mach number. It should be noted that b_s is the half-chord of the wing taken at the intersection of the wing and fuselage.

RESULTS AND DISCUSSION

General comments.- Visual observations, examination of high-speed-camera results, and comparison of flutter frequencies with natural frequencies indicated that the flutter obtained in the current tests was most probably of the classical bending-torsion type. A sequence of views of flutter on two swept wings is presented in figure 6. One sequence shows the 445 wing viewed from a position downstream of and slightly below the wing; the other sequence shows the 460 wing viewed from a position upstream of and slightly above the wing. These edge-on views give some indication of the mode shape during flutter. Observation of the 460 wing, which has a higher length-chord ratio than the 445 wing, shows that the mode shape in bending is characterized by an outward displacement from the wing root of the region of maximum curvature. This shape suggests the presence of components of natural bending modes higher than the first in the flutter mode and therefore suggests that perhaps higher modes should be considered in the analytical representation of the flutter mode.

Observation and time records of strain-gage traces showed that in the majority of cases both wing panels of each wing fluttered almost simultaneously. In the few cases where simultaneous flutter did not occur on both wing panels, a separate point is presented in the results for the beginning of flutter on each panel.

The results of the investigation are presented in table III and figures 7 to 10. Table III contains the values at flutter of the pertinent physical quantities such as experimental flutter speed V_e, and parameters such as mass-density ratio μ and flutter-speed coefficient $V_e/b_r\omega_\alpha$. Also given are the values of the calculated reference flutter speed V_R. In the figures, V_R is used as a normalizing factor in the graphical presentation of the experimental flutter speeds.

Effects of sweep on flutter-speed ratio.- The effects of sweepback on the variation of flutter-speed ratio with Mach number for wings with an aspect ratio of 4 and sweepback of 0°, 45°, 52.5°, and 60° are shown in figures 7 and 8. The curves of V_e/V_R against Mach number, presented in figure 7, are well-defined by many data points for the 0°, 52.5°, and 60° sweep angles. The curve for 45° sweep lacks points between Mach numbers of 1.0 and 1.4 and, as a consequence, the fairing of the curve in this region is somewhat arbitrary. More data are needed for the 60° sweep curve below Mach number 1.0. The curve is extrapolated, however, along a reasonable path to a Mach number of 0.8 as shown by the dotted line.

There is an indication of a variation with sweep angle of the values of V_e/V_R at Mach numbers less than 1.0. The calculated flutter speeds at these Mach numbers are fairly close to the experimental values for the wings of 0°, 45°, and 52.5° sweepback; whereas a somewhat greater difference between theoretical and experimental values is indicated for the wing of 60° sweepback. A similar trend in the magnitude of the variation of V_e/V_R with sweep at moderate subsonic Mach numbers is shown in reference 2, figure 15. The actual values of V_e/V_R in figure 7 are, however, lower than the values of reference 2.

In order to show more clearly the effect of sweepback on the variation of flutter-speed ratio with Mach number, the curves of figure 7 have been normalized by dividing each value of V_e/V_R by the value of V_e/V_R at a Mach number of 0.8. These normalized curves are presented in figure 8. The curves show that the favorable increase in flutter-speed ratio with Mach number in the transonic and low supersonic range is less pronounced as the sweep angle is increased; that is, the compressibility effect, although first appearing at about the same Mach number for each wing, is consistently less for the more highly swept wings.

Effects of aspect ratio on flutter-speed ratio.- The effect of aspect ratio on the flutter-speed ratio for the wings of 45° sweepback is shown

[redacted]

in figures 9 and 10. The flutter-speed ratio V_e/V_R is plotted against Mach number in figure 9 for wings having aspect ratios of 2, 4, and 6. There is a significant decrease in V_e/V_R with increasing aspect ratio at Mach numbers of the order of 0.8. The values of V_e/V_R are 1.52, 1.0, and 0.77 for aspect ratios of 2, 4, and 6, respectively. This variation of V_e/V_R with aspect ratio is in agreement with trends shown in reference 3, particularly for the lower aspect ratio wings. It should perhaps be pointed out that the relatively high values of V_e/V_R noted for the aspect-ratio-2 wing may be attributable in part to differences in the method of obtaining the elastic-axis position of the 245 wing as compared to that for the other wings. As mentioned previously, the manner of clamping this wing in the experimental determination of the elastic-axis position, resulted in a comparatively far rearward elastic-axis position with consequent large values of $(r_\alpha)^2$ and $|x_\alpha|$. A sample V_R calculation for the 245 wing employing an assumed elastic-axis position and effective root chord definition similar to that of the other wings, with corresponding values of $(r_\alpha)^2$ and x_α, gave values of V_e/V_R approximately 10 percent less than the values shown in figure 9. The unconservative values of V_R as shown in figure 9 for the wing of aspect ratio 6 are disturbingly high and, as yet, no satisfactory explanation can be given for the degree of unconservatism. One possibility is that the inclusion of higher modes in the analysis than first bending and first torsion may lower the values of V_R. Some thought has also been given to the possibility that the flutter encountered on the 645 wing was of the single-degree-of-freedom bending type described in references 4 and 5. This possibility seems unlikely, however, on the basis of the curves given in figure 3 of reference 4.

The curves of figure 10 are the curves of figure 9 normalized with the value of V_e/V_R at a Mach number of 0.8. Since the curves nearly coincide, they indicate that the variation with Mach number of the flutter-speed ratio in the transonic and low supersonic range is practically the same for aspect ratios 2, 4, and 6.

Application of results.- In this section an application is made of the curves of V_e/V_R to obtain curves of flutter-speed coefficient, $V'/b_s\omega_\alpha$ against Mach number for a given value of mass-density ratio μ. The curves of $V'/b_s\omega_\alpha$ as a function of M_e, which are presented in figures 11 and 12, give an indication of the effect of wing-plan-form geometry on the variation of the flutter-speed coefficient with Mach number. Some of the differences between the curves for the various wing plan forms is also attributable to variations in certain of the physical parameters which describe the wings. Perhaps the most significant difference in the physical properties of the wings is found in the bending-torsion frequency ratio which varies from about 0.36 to about 0.098 as the sweepback of the aspect-ratio-4 wings is varied from 0° to 60°, and which varies from about 0.65 to about 0.09 as the aspect ratio of the 45° sweptback wing varies from 2 to 6. The comparison of wing plan forms

shown in figures 11 and 12 is, therefore, one in which changes in frequency ratio accompany changes in wing-plan-form geometry. The direction in which the frequency ratio changes with plan-form geometry for the curves shown in figures 11 and 12 is perhaps the same, however, as might be expected on actual airplane wings without external appendages.

Comparison of the curves of figures 11 and 12 indicates that for a given root chord and torsional frequency there is a relatively small effect of sweep on the flutter speed for Mach numbers less than 1.0. At higher Mach numbers, however, there is a large systematic effect of sweepback on the flutter speed with the straight wing having the highest flutter speed. The curves of figure 12 show that for the same root chord and torsional frequency, there is a very large increase in flutter speed as the aspect ratio is decreased from 4 to 2, but that a relatively small increase in flutter speed accompanies a reduction in aspect ratio from 6 to 4. These comparisons are made on the basis of a fixed torsional frequency and chord length as the plan form is varied. In practice, however, it would seem likely that the torsion frequency would vary with plan form. In any case, the comparative values of the actual flutter speed for the wings of different plan form will obviously vary with the torsion frequency. Again, the differences in the method of obtaining the elastic-axis position for the 245 wing should perhaps be considered in comparing the values of flutter-speed coefficient for the 245 wing with the values for the other wings tested. In the case of the flutter-speed coefficient $V'/b_s\omega_\alpha$, the effect of the rearward location of the elastic axis obtained for the 245 wing is evident in the low values of ω_α resulting from the use of the relatively large values of $|x_\alpha|$ in the formula for the uncoupled frequency.

It should be emphasized that the comparisons of the effect of plan form on the flutter speed as shown in figures 11 and 12 are based on wings which are characterized by particular values of the various pertinent physical parameters such as frequency ratio and center-of-gravity position. Changes in the values of these parameters for one wing with respect to another would, of course, alter these comparisons. For example, a rearward movement of the center-of-gravity position of the straight wing would lower the flutter speed of this wing with respect to the flutter speeds of the swept wings.

The manner in which the curves of figures 11 and 12 were obtained illustrates the application of the curves of V_e/V_R given in figures 7 and 9. Caution should be exercised, however, in applying these flutter-speed ratios to the determination of the flutter speed of wings which have values of ω_h/ω_α, x_α, a, r_α, and μ much different from those which characterize the wings of the present investigation. It might be hoped that the reference-flutter-speed calculations, as obtained in the present paper, have adequately removed from the results the effects of such variables as the center-of-gravity position, and that the curves of

V_e/V_R against Mach number are a function of plan form only. It is not entirely evident, however, that such is the case and it is thought that further investigation of particular wing plan forms having different values of the various pertinent parameters which go into the reference-speed calculation are required in order to establish the applicability of the results obtained.

CONCLUSIONS

The results of a systematic study of the effects of variation in wing plan form on flutter at transonic speeds indicated:

1. The flutter-speed ratio increased rapidly past sonic speed for sweep angles of 45° and less, indicating a favorable effect of Mach number. For sweepback of 60°, the flutter-speed ratio was nearly constant throughout the Mach number range of the tests.

2. Reducing the aspect ratio had a favorable effect on the flutter-speed ratio which was of the order of 100 percent higher for the aspect-ratio-2 wing than for the aspect-ratio-6 wing. This percentage difference was nearly constant throughout the Mach number range, indicating that the effect of Mach number was about the same for all aspect ratios tested.

3. Further investigation is needed to establish the generality of the results employing the reference flutter speed as a normalizing factor.

Langley Aeronautical Laboratory,
National Advisory Committee for Aeronautics,
Langley Field, Va., June 18, 1953.

REFERENCES

1. Bursnall, William J.: Initial Flutter Tests in the Langley Transonic Blowdown Tunnel and Comparison With Free-Flight Flutter Results. NACA RM L52K14, 1953.

2. Barmby, J. G., Cunningham, H. J., and Garrick, I. E.: Study of the Effects of Sweep on the Flutter of Cantilever Wings. NACA Rep. 1014, 1951. (Supersedes NACA TN 2121.)

3. Widmayer, E., Jr., Lauten, W. T., Jr., and Clevenson, S. A.: Experimental Investigation of the Effect of Aspect Ratio and Mach Number on the Flutter of Cantilever Wings. NACA RM L50C15a, 1950.

4. Cunningham, H. J.: Analysis of Pure-Bending Flutter of a Cantilever Swept Wing and Its Relation to Bending-Torsion Flutter. NACA TN 2461, 1951.

5. Regier, Arthur A., and Martin, Dennis J.: Recent Experimental Flutter Studies. NACA RM L51F11, 1951.

TABLE I.- WING PARAMETERS

Parameter	Wing					
	245	400	445	452	460	645
NACA section	65A004	65A004	65A004	65A004*	65A004*	65A004
A	2	4	4	4	4	6
Λ, deg	45	0	45	52.5	60	45
λ	0.6	0.6	0.6	0.6	0.6	0.6
Panel λ	0.685	0.657	0.657	0.657	0.657	0.646
Span, ft	0.808	1.142	1.142	1.142	1.142	1.400
A_g	0.91	1.65	1.65	1.65	1.65	2.75
l, ft	0.306	0.445	0.630	0.732	0.892	0.813
b_r, ft	0.129	0.163	0.123	0.107	0.086	0.094
b_s, ft	0.183	0.163	0.163	0.163	0.163	0.127
f_{h_1}, cps	135	147	88	61	35	46
f_{h_2}, cps	630	630	462	300	198	227
f_t, cps	425	407	370	370	370	522
f_α, cps	208	402	361	366	362	505
$(\omega_h/\omega_\alpha)^2$	0.420	0.133	0.0531	0.0282	0.0093	0.0083
μ_{stnd} at 0.75η	20.89	36.57	51.43	69.29	102.94	74.35
g_h	0.023	0.020	0.030	0.021	0.027	0.013

* Approximate section - actual section about 5 percent thick.

TABLE II.- WING PARAMETERS AT SPANWISE STATIONS

η	Wing 245				Wing 400				Wing 445			
	x_α	a	r_α^2	m, slugs/ft	x_α	a	r_α^2	m, slugs/ft	x_α	a	r_α^2	m, slugs/ft
0.05	-0.64	0.53	0.66	0.00217	0.14	-0.23	0.24	0.00738	-0.02	-0.07	0.22	0.00561
.15	- .66	.55	.69	.00207	.12	- .22	.25	.00716	+0.01	- .10	.22	.00527
.25	- .68	.57	.72	.00198	.11	- .21	.26	.00671	.04	- .13	.23	.00493
.35	- .70	.59	.74	.00189	.09	- .19	.27	.00617	.07	- .15	.24	.00458
.45	- .72	.61	.77	.00179	.08	- .18	.28	.00563	.09	- .18	.24	.00424
.55	- .74	.63	.80	.00170	.06	- .16	.28	.00509	.12	- .21	.25	.00389
.65	- .76	.65	.83	.00161	.05	- .15	.28	.00455	.15	- .24	.26	.00355
.75	- .78	.67	.86	.00152	.03	- .13	.27	.00400	.17	- .26	.26	.00321
.85	- .80	.69	.89	.00143	.02	- .11	.25	.00345	.20	- .29	.27	.00286
.95	- .82	.71	.92	.00134	.004	- .10	.24	.00291	.23	- .32	.28	.00252

η	Wing 452				Wing 460				Wing 645			
	x_α	a	r_α^2	m, slugs/ft	x_α	a	r_α^2	m, slugs/ft	x_α	a	r_α^2	m, slugs/ft
0.05	+0.37	-0.44	0.27	0.00573	+0.21	-0.31	0.26	0.00465	0.15	-0.25	0.26	0.00480
.15	.30	- .37	.27	.00538	.14	- .23	.24	.00438	.15	- .24	.26	.00437
.25	.24	- .31	.29	.00503	.07	- .16	.23	.00410	.14	- .23	.25	.00404
.35	.17	- .24	.32	.00468	-0.004	- .09	.23	.00383	.13	- .23	.25	.00381
.45	.11	- .18	.29	.00433	- .08	- .02	.24	.00356	.13	- .22	.24	.00362
.55	.04	- .11	.27	.00398	- .15	+0.05	.27	.00334	.12	- .21	.24	.00335
.65	-0.02	- .05	.27	.00363	- .22	.12	.30	.00320	.11	- .21	.24	.00302
.75	- .09	+0.02	.28	.00328	- .29	.19	.35	.00314	.11	- .20	.25	.00266
.85	- .15	.08	.30	.00293	- .36	.26	.43	.00301	.10	- .20	.28	.00243
.95	- .22	.15	.31	.00258	- .43	.33	.51	.00283	.10	- .19	.33	.00226

TABLE III.- EXPERIMENTAL AND ANALYTICAL RESULTS

(a) MODEL - 245 MATERIAL - PINE-BALSA

ρ_e	μ_e $\eta=.75$	q_e	ω_e	ω_R	ω_e/ω_R	V_e	$V_e/b_r\omega_\alpha$	V_R	V_e/V_R	M_e
.0042	12.0	1522	1748	1610	1.086	851	5.037	574	1.483	.846
.0041	12.2	1720	1690	1607	1.052	916	5.420	579	1.581	.908
.0033	15.2	1687	1532	1564	.980	1011	5.981	630	1.604	1.012
.0029	17.3	1599	1520	1540	.987	1050	6.213	663	1.584	1.056
.0033	15.2	1958	1785	1564	1.142	1089	6.446	630	1.728	1.116
.0029	17.3	1768	1555	1540	1.010	1104	6.533	663	1.666	1.120
.0031	16.2	1860	1790	1552	1.153	1096	6.482	646	1.696	1.128
.0035	14.3	2295	1854	1577	1.175	1145	6.776	616	1.859	1.204
.0041	12.2	2715	1954	1607	1.216	1151	6.810	579	1.987	1.230
.0047	10.7	2420	1802	1631	1.105	1015	6.004	550	1.846	1.244
.0038	13.2	2667	2003	1592	1.258	1185	7.010	597	1.986	1.281
.0041	12.2	2946	2018	1607	1.256	1199	7.093	579	2.069	1.298

(b) MODEL - 400 MATERIAL - COMPREG WOOD

ρ_e	μ_e $\eta=.75$	q_e	ω_e	ω_R	ω_e/ω_R	V_e	$V_e/b_r\omega_\alpha$	V_R	V_e/V_R	M_e
.0029	30	966	1110	1553	.715	816	1.98	936	.872	.809
.0040	22	1275	1147	1582	.725	799	1.94	811	.985	.809
.0032	27	1088	1047	1560	.671	825	2.00	896	.921	.833
.0032	27	1132	1066	1560	.683	841	2.04	896	.939	.852
.0035	25	1234	1152	1570	.734	840	2.04	860	.976	.855
.0028	31	1103	1154	1548	.745	888	2.16	951	.934	.884
.0026	33	1004	1047	1541	.679	879	2.13	983	.893	.886
.0028	31	1149	1079	1549	.696	906	2.20	951	.953	.918
.0029	30	1220	1105	1553	.712	917	2.23	936	.980	.938
.0028	31	1192	--	1549	--	923	2.24	951	.971	.943
.0025	35	1141	1131	1534	.737	955	2.32	1001	.954	.968
.0027	32	1220	1092	1544	.707	951	2.31	966	.984	.975
.0027	32	1296	1230	1544	.797	980	2.38	965	1.015	.990
.0025	35	1198	1120	1534	.730	979	2.38	1001	.978	1.005
.0026	33	1260	1123	1541	.729	985	2.39	983	1.001	1.016
.0024	36	1358	1068	1532	.697	1064	2.58	1020	1.043	1.114
.0029	30	1858	1314	1553	.846	1132	2.75	936	1.210	1.192
.0039	22	2430	1414	1581	.894	1116	2.71	820	1.361	1.232
.0031	28	2053	1356	1559	.870	1151	2.79	908	1.267	1.259
.0034	26	2254	1482	1568	.945	1151	2.80	871	1.322	1.278
.0031	28	2197	1417	1558	.910	1191	2.89	908	1.311	1.322
.0040	22	2802	1487	1583	.940	1184	2.87	811	1.459	1.324
.0035	25	2724	1468	1570	.935	1248	3.03	860	1.450	1.346

NACA

TABLE III. - Continued

(c) MODEL - 445 MATERIAL - COMPREG WOOD

ρ_e	μ_e η=.75	q_e	ω_e	ω_R	ω_e/ω_R	V_e	$V_e/b_r\omega_\alpha$	V_R	V_e/V_R	M_e
.0028	47	903	1063	1167	.911	803	2.88	850	.945	.794
.0031	43	981	1047	1187	.882	796	2.85	819	.972	.797
.0031	39	981	1047	1221	.857	796	2.85	818	.972	.797
.0033	37	1070	1047	1239	.845	805	2.89	799	1.008	.813
.0028	47	1026	995	1167	.852	856	3.07	850	1.007	.863
.0028	47	1013	--	1167	--	851	3.05	850	1.001	.863
.0028	44	1026	995	1196	.832	856	3.07	850	1.007	.863
.0027	49	1067	958	1167	.821	889	3.19	865	1.028	.904
.0026	51	1024	995	1157	.860	888	3.18	875	1.014	.906
.0024	55	1009	1059	1137	.932	917	3.29	899	1.020	.908
.0024	51	1009	1120	1157	.968	917	3.29	893	1.027	.908
.0025	53	1056	1040	1148	.906	919	3.29	888	1.035	.921
.0025	49	1055	1040	1173	.887	919	3.29	882	1.042	.921
.0027	49	985	1162	1167	.996	854	3.06	865	.988	.924
.0020	61	1005	1091	1115	.978	1003	3.59	956	1.048	.961
.0024	55	1155	1121	1137	.986	981	3.52	899	1.091	.972
.0024	51	1155	1158	1157	1.001	981	3.52	893	1.099	.972
.0020	61	994	1118	1115	1.002	997	3.57	956	1.042	1.004
.0029	42	2406	1503	1202	1.251	1288	4.62	838	1.537	1.386

(d) MODEL - 452 MATERIAL - COMPREG WOOD

ρ_e	μ_e η=.75	q_e	ω_e	ω_R	ω_e/ω_R	V_e	$V_e/b_r\omega_\alpha$	V_R	V_e/V_R	M_e
.0049	34	1175	1032	1257	.821	693	2.81	842	.823	.787
.0035	47	1171	1016	1172	.867	818	3.31	958	.854	.795
.0042	39	1343	1037	1218	.851	800	3.22	887	.901	.803
.0028	59	1177	906	1118	.810	917	3.72	1040	.882	.892
.0030	55	1366	1062	1134	.936	954	3.84	1005	.949	.995
.0029	57	1365	1068	1126	.949	970	3.90	1018	.954	1.003
.0030	55	1384	1062	1134	.936	961	3.86	1005	.955	1.003
.0028	59	1319	1068	1117	.956	971	3.90	1031	.942	1.005
.0027	61	1407	953	1110	.859	1021	4.14	1054	.969	1.018
.0024	69	1338	916	1080	.848	1056	4.28	1099	.960	1.060
.0024	69	1392	942	1080	.872	1077	4.36	1099	.980	1.087
.0025	66	1358	1049	1089	.964	1042	4.19	1073	.971	1.102
.0024	69	1446	1062	1079	.984	1098	4.41	1088	1.009	1.175
.0026	63	1622	1100	1099	1.000	1117	4.49	1058	1.056	1.206
.0022	71	1508	1093	1057	1.034	1171	4.71	1122	1.044	1.265
.0026	63	2078	1136	1100	1.033	1264	5.12	1068	1.184	1.398
.0026	63	2179	1120	1100	1.018	1295	5.25	1068	1.212	1.425

NACA

[redacted]

TABLE III.- Concluded

(e) MODEL - 460 MATERIAL - COMPREG WOOD

ρ_e	μ_e η=.75	q_e	ω_e	ω_R	ω_e/ω_R	V_e	$V_e/b_r\omega_\alpha$	V_R	V_e/V_R	M_e
.0028	87	1409	792	983	.806	1005	5.14	1250	.803	1.024
.0032	77	1534	823	1013	.813	985	5.04	1200	.821	1.038
.0032	77	1533	873	1013	.862	983	5.03	1200	.821	1.038
.0032	77	1590	848	1013	.838	1005	5.14	1200	.837	1.048
.0031	79	1558	829	1007	.821	996	5.09	1207	.829	1.058
.0031	79	1533	873	1007	.869	1001	5.12	1207	.825	1.064
.0032	77	1676	886	1013	.873	1025	5.24	1200	.857	1.076
.0028	87	1500	823	983	.836	1033	5.28	1250	.827	1.112
.0029	85	1564	867	991	.875	1039	5.31	1236	.840	1.119
.0024	103	1436	861	946	.910	1096	5.60	1319	.831	1.175
.0023	109	1489	836	933	.896	1148	5.87	1343	.854	1.241
.0023	109	1489	873	933	.936	1148	5.87	1343	.854	1.241
.0021	115	1488	873	918	.951	1182	6.04	1375	.860	1.289
.0020	124	1479	811	899	.900	1222	6.25	1402	.872	1.316
.0020	124	1517	873	899	.972	1241	6.34	1402	.885	1.371

(f) MODEL - 645 MATERIAL - MAGNESIUM

ρ_e	μ_e η=.75	q_e	ω_e	ω_R	ω_e/ω_R	V_e	$V_e/b_r\omega_\alpha$	V_R	V_e/V_R	M_e
.0043	41	1154	1047	1576	.665	733	2.45	1007	.727	.730
.0042	42	1323	767	1569	.489	794	2.65	1018	.780	.783
.0038	46	1305	1023	1540	.664	829	2.77	1061	.781	.832
.0036	49	1239	1063	1525	.697	830	2.77	1085	.765	.832
.0035	50	1240	1058	1518	.697	842	2.81	1098	.767	.846
.0033	53	1271	943	1501	.628	878	2.93	1124	.780	.890
.0034	52	1363	1047	1509	.694	896	2.99	1111	.806	.911
.0028	63	1333	1049	1455	.721	976	3.26	1203	.811	1.008
.0027	65	1309	1018	1446	.704	985	3.29	1220	.807	1.012
.0025	71	1239	961	1424	.675	995	3.32	1259	.791	1.022
.0030	59	1443	1049	1474	.712	984	3.29	1169	.842	1.033
.0025	71	1274	942	1424	.661	1009	3.37	1259	.802	1.038
.0024	74	1309	1005	1413	.711	1044	3.49	1280	.816	1.062
.0028	63	1527	1382	1455	.950	1044	3.49	1203	.868	1.085
.0028	63	1743	1131	1455	.777	1116	3.73	1203	.928	1.237
.0035	50	2378	1319	1518	.869	1166	3.89	1098	1.062	1.266
.0038	46	2575	1366	1540	.887	1164	3.89	1061	1.097	1.278
.0040	44	2721	1370	1554	.882	1166	3.90	1039	1.123	1.284
.0032	55	2285	1225	1491	.822	1195	3.99	1138	1.050	1.284
.0036	49	2530	1370	1525	.899	1186	3.96	1085	1.093	1.296
.0035	50	2589	1313	1518	.865	1216	4.06	1098	1.108	1.322

NACA

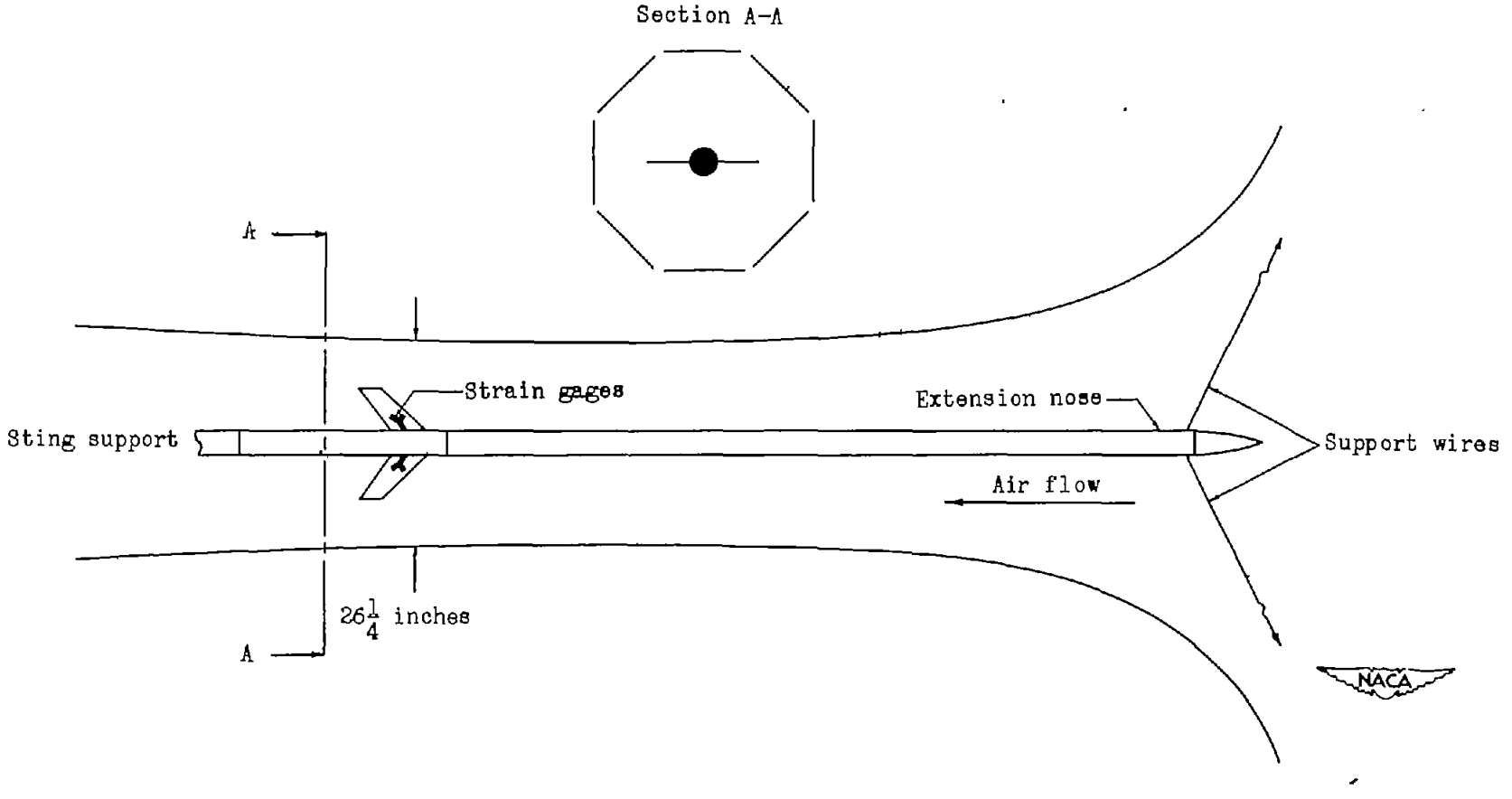

Figure 1.- Plan view of Langley transonic blowdown tunnel with flutter model installed.

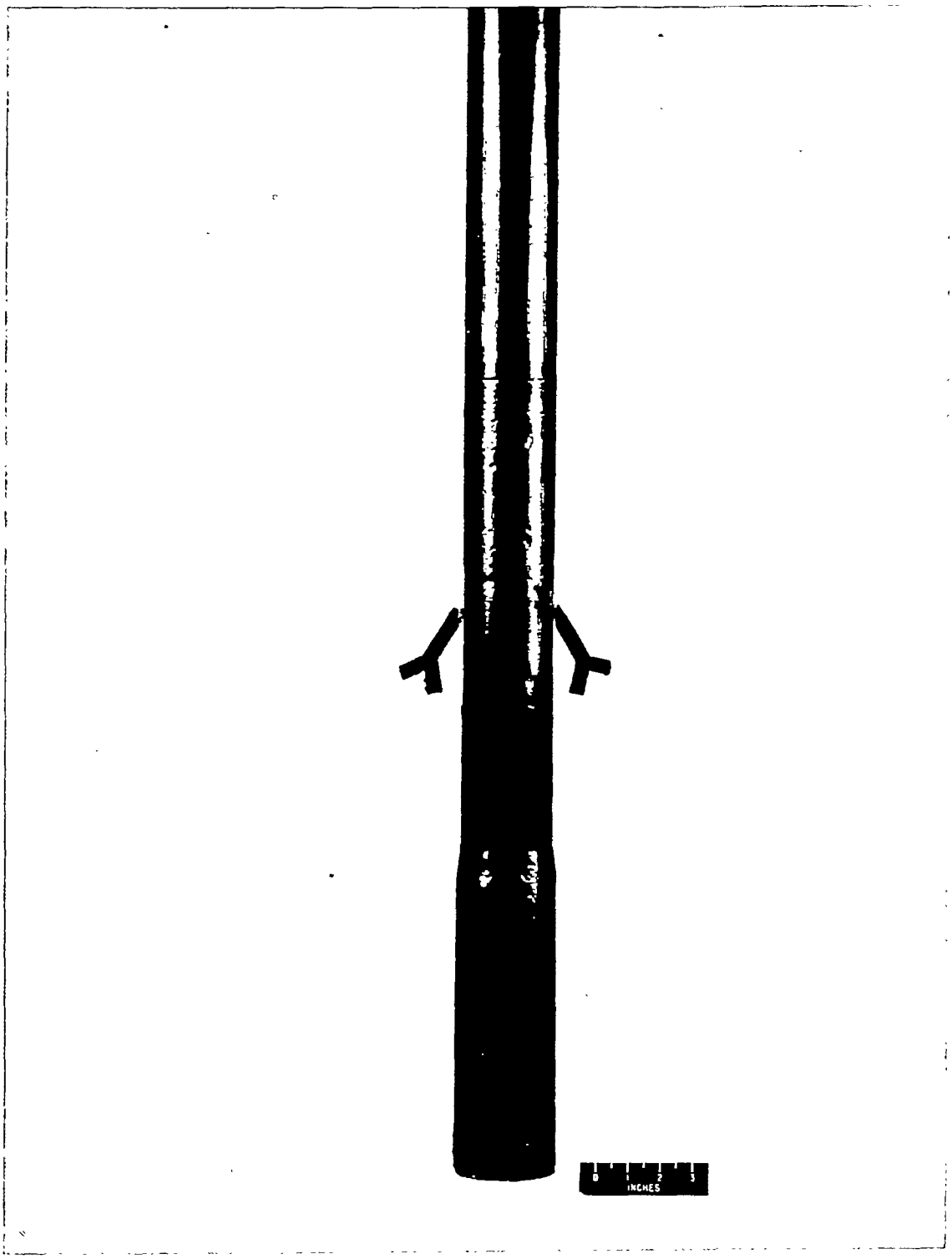

NACA L-79715.1

Figure 2.- Flutter model of a wing with an aspect ratio of 4 and 60° of sweepback, mounted on sting fuselage.

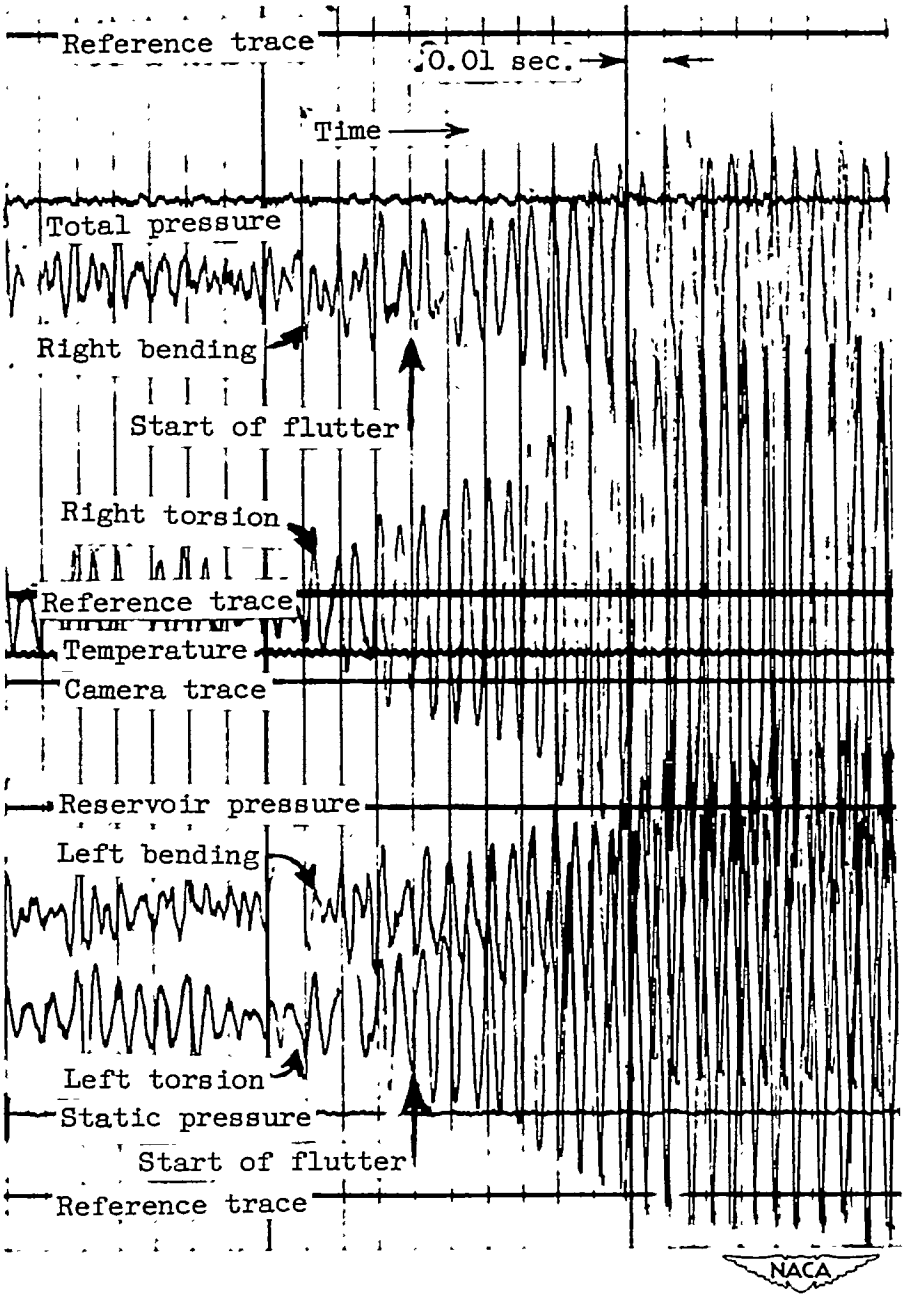

Figure 3.- Sample oscillograph record of flutter test. (Wing 445 at M = 0.813.)

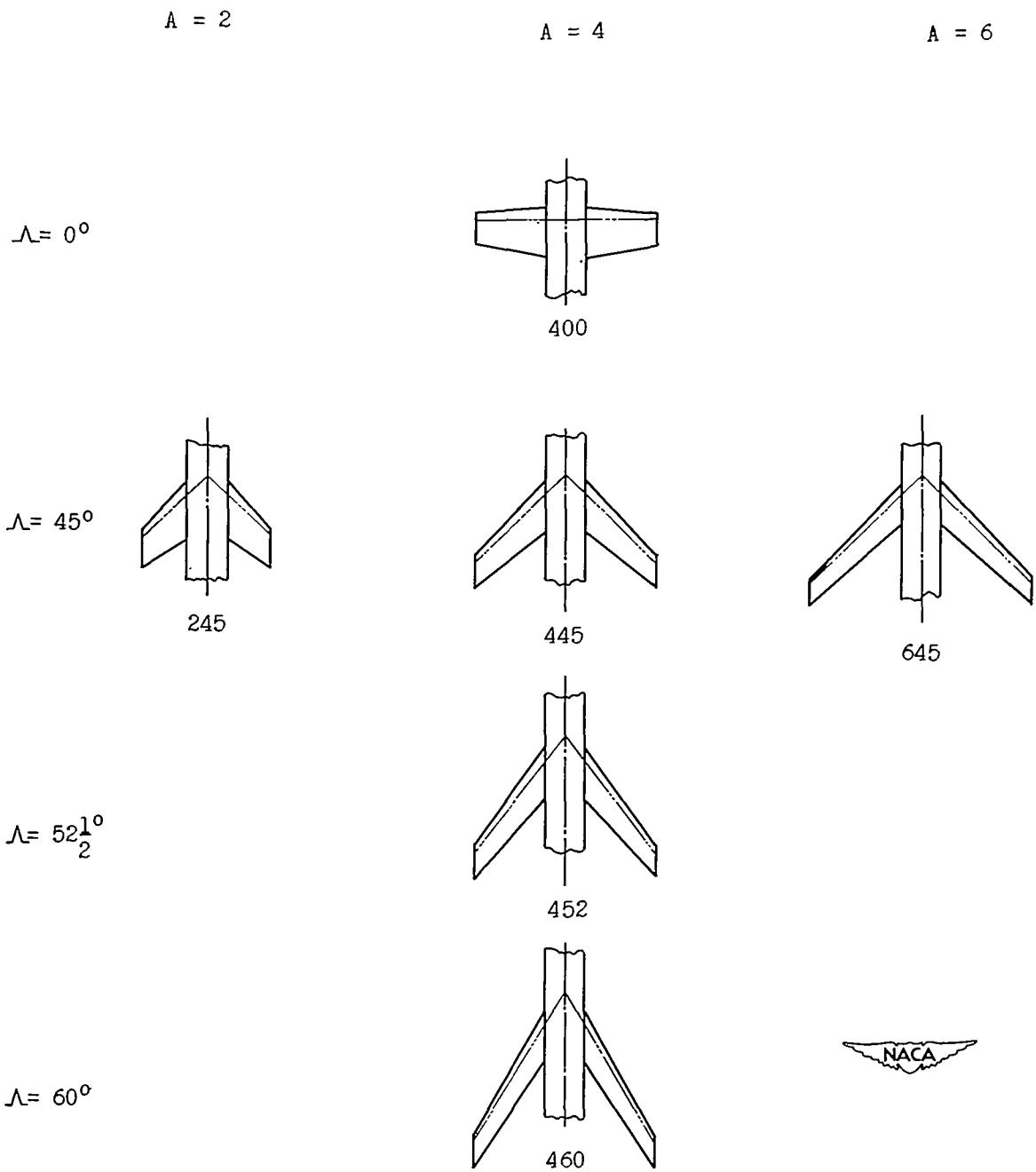

Figure 4.- Plan forms of flutter models giving aspect ratio, sweep angle, and model designations.

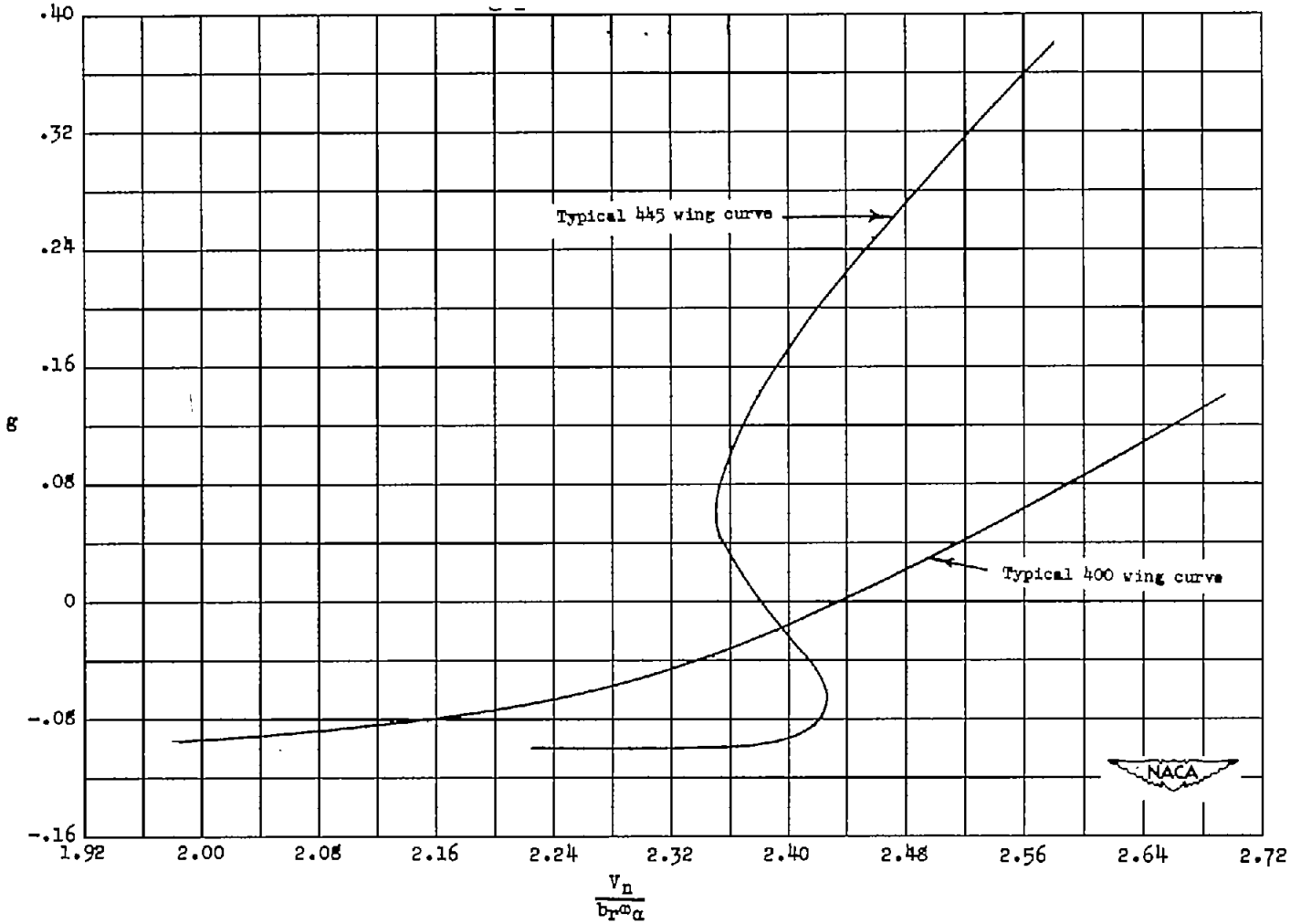

Figure 5.- Typical curves of structural damping g against the parameter $\frac{V_n}{b_r \omega_\alpha}$.

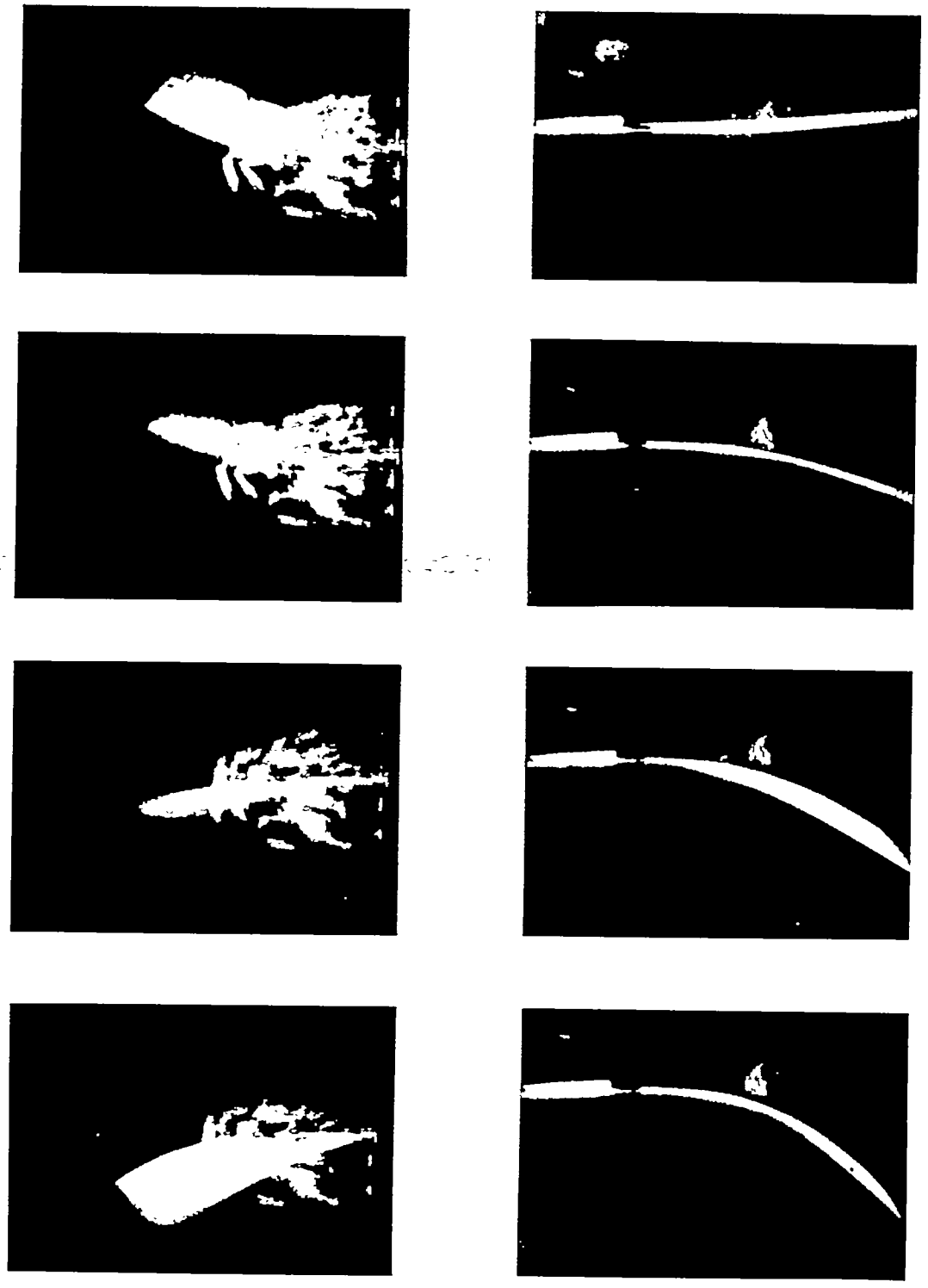

445 wing 460 wing L-80289

Figure 6.- Sequences from high-speed motion pictures of flutter of 445 and 460 wings.

[redacted]

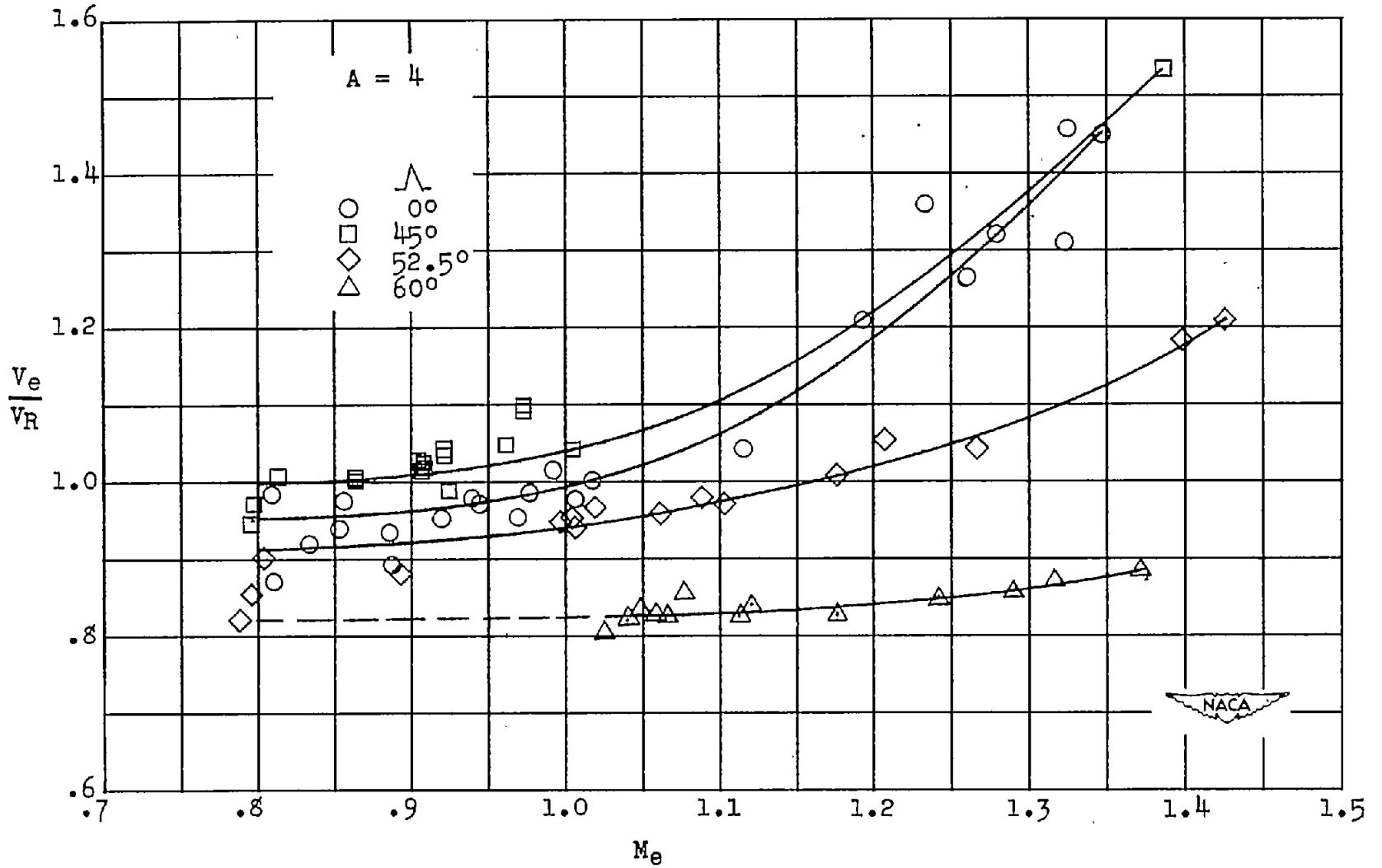

Figure 7.- Effect of sweepback on variation of flutter-speed ratio with Mach number for aspect-ratio-4 wings.

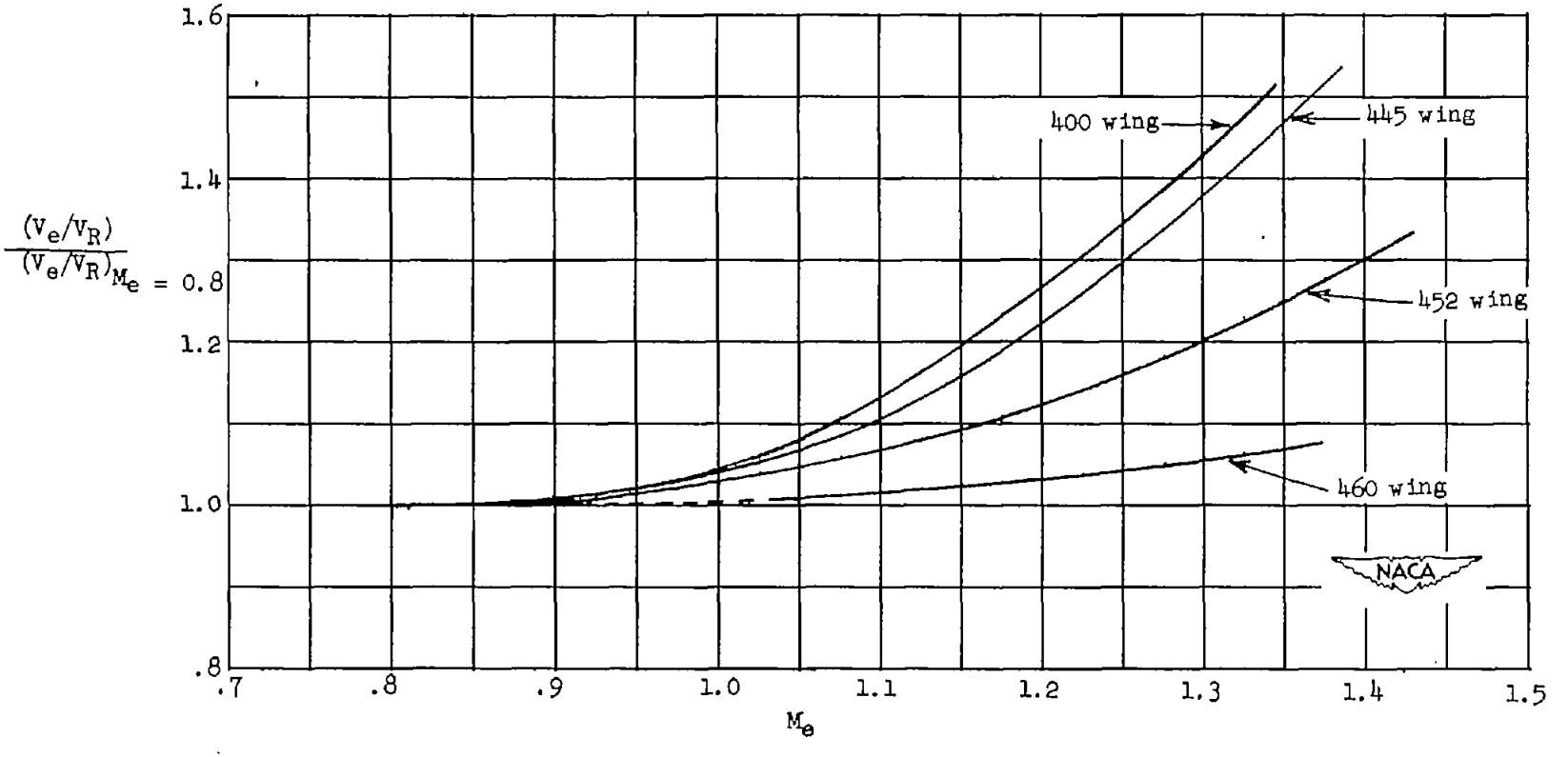

Figure 8.- Effect of sweepback on variation of normalized flutter-speed ratio with Mach number for aspect-ratio-4 wings.

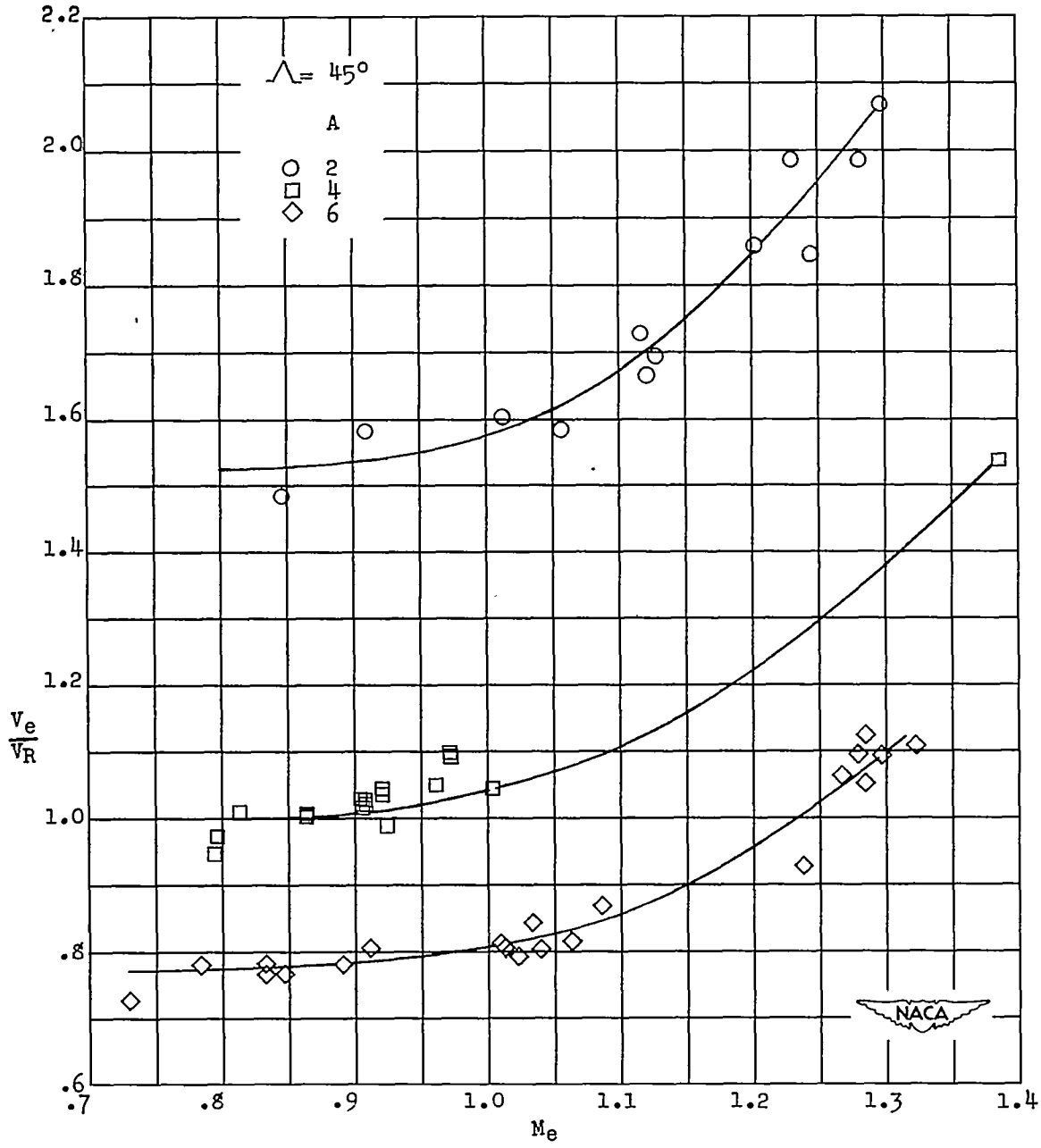

Figure 9.- Effect of aspect ratio on variation of flutter-speed ratio with Mach number for wings with 45° sweepback.

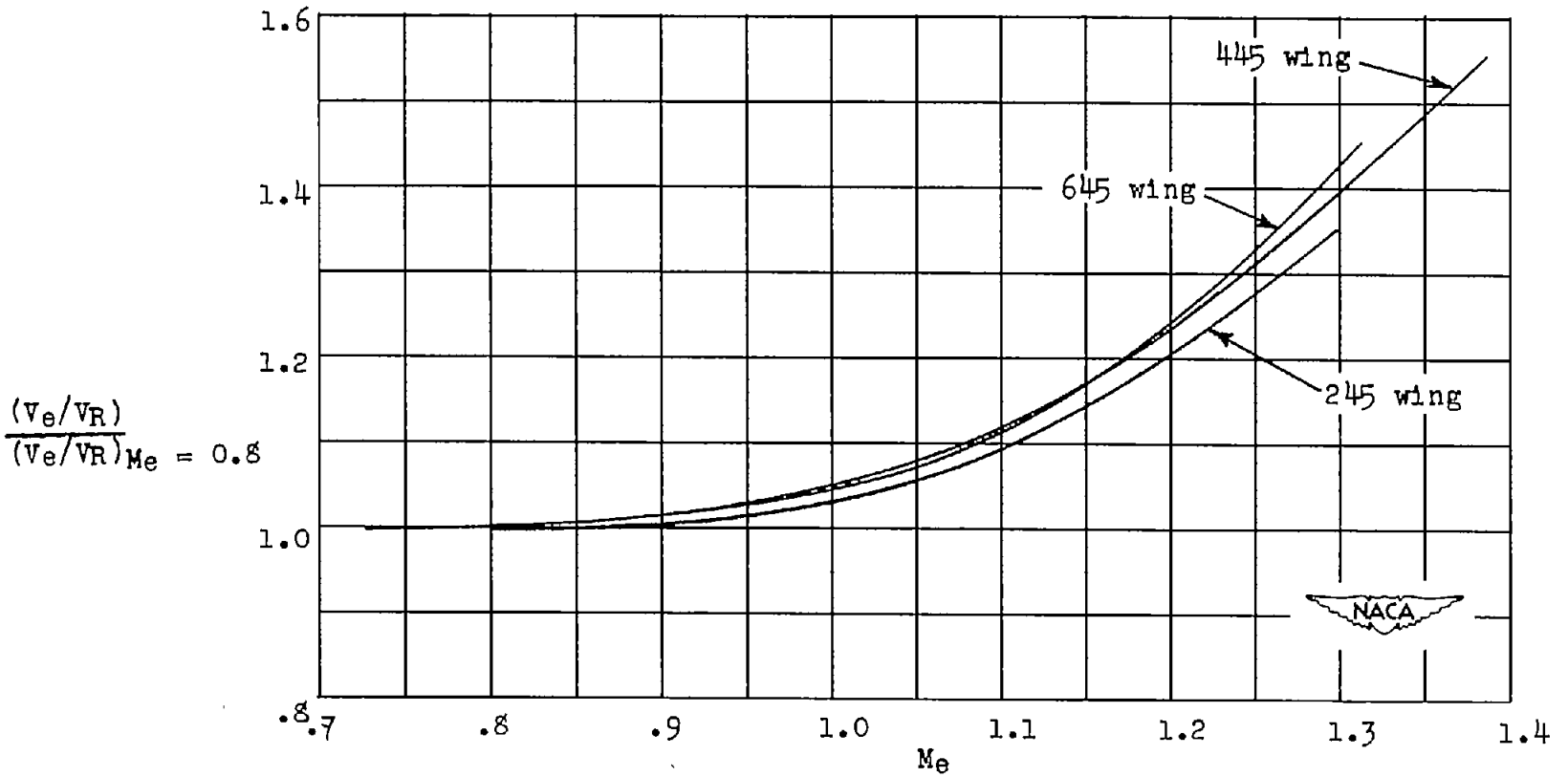

Figure 10.- Effect of aspect ratio on variation of normalized flutter-speed ratio with Mach number for wings with 45° sweepback.

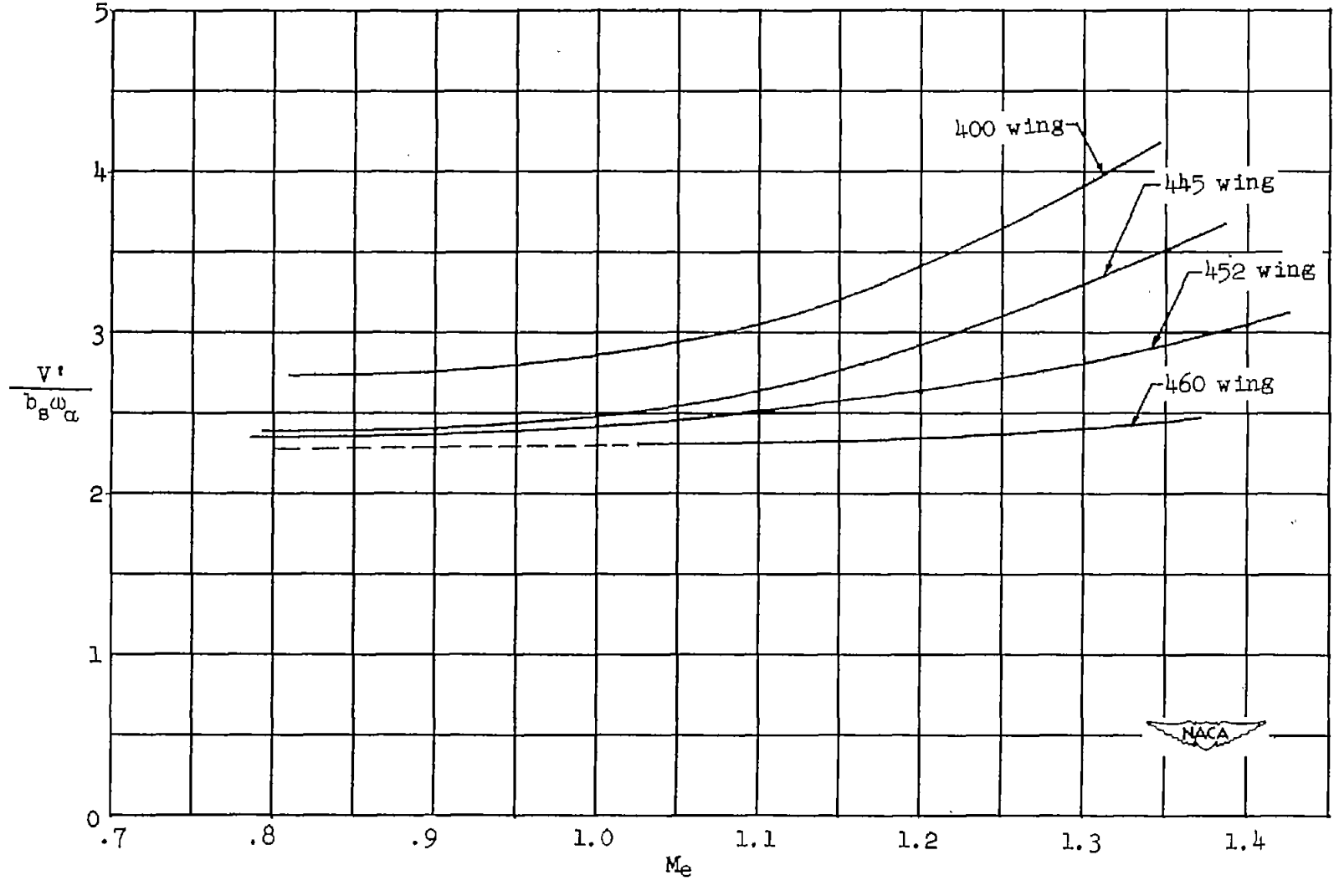

Figure 11.- Effect of sweepback on variation of estimated flutter-speed coefficient with Mach number for aspect-ratio-4 wings. $\mu = 50$.

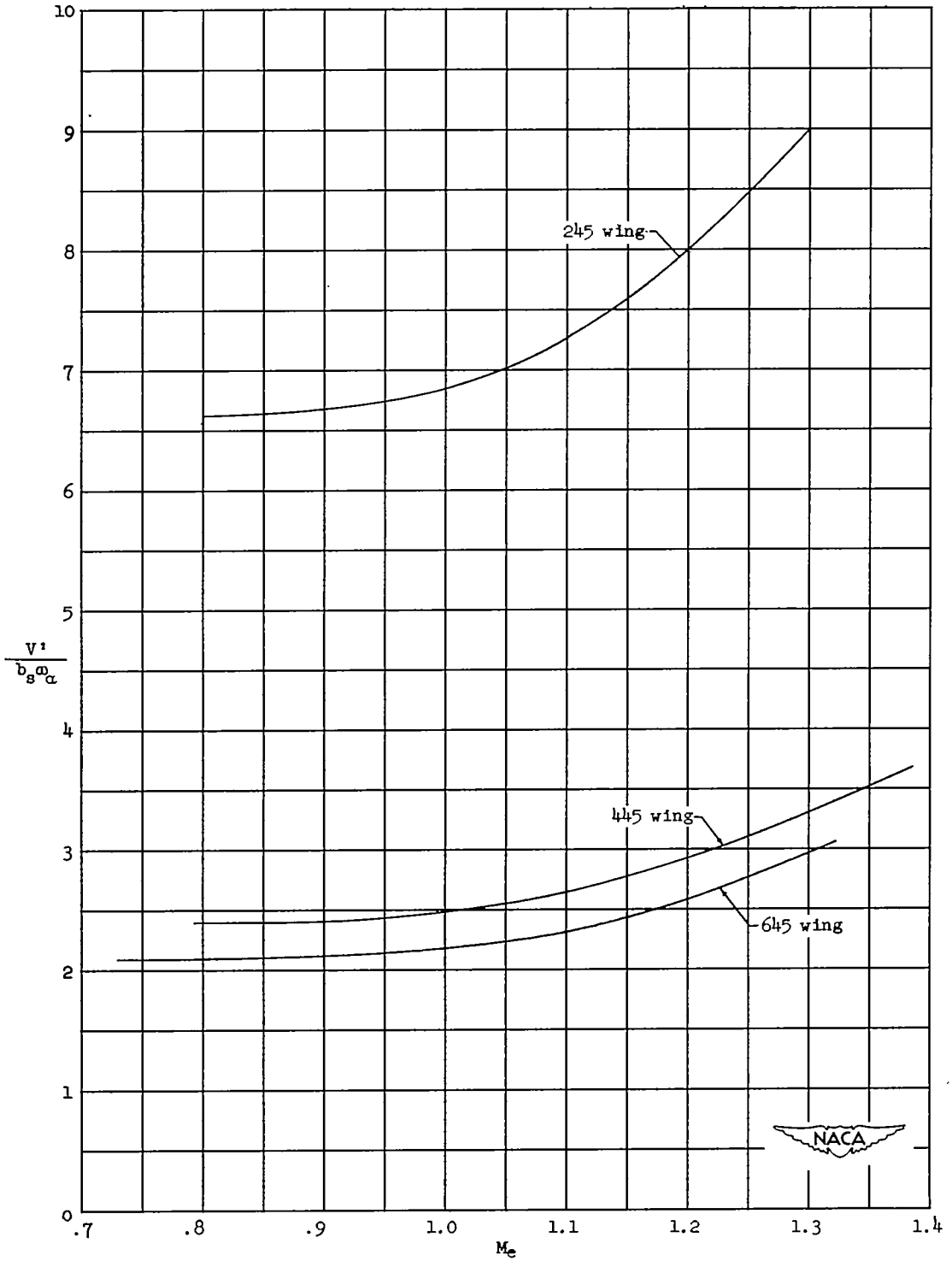

Figure 12.- Effect of aspect ratio on variation of flutter-speed coefficient with Mach number for wings with 45° sweepback. $\mu = 50$.

NACA-Langley - 8-13-53 - 325